catalysts

MDPI

Article

Yttria-Stabilized Zirconia of Balanced Acid-Base Pair for Selective Dehydration of 4-Methyl-2-pentanol to 4-Methyl-1-pentene

Jae-Hong Lee [1], Minseok Kim [1], Suhyun Lim [1], Dinesh Kumar Mishra [1,2] and Young-Woong Suh [1,2,*]

[1] Department of Chemical Engineering, Hanyang University, Seoul 04763, Korea; classicjae@hanyang.ac.kr (J.-H.L.); im.mkim87@gmail.com (M.K.); lim03187@naver.com (S.L.); rdineshvns@gmail.com (D.K.M.)
[2] Research Institute of Industrial Science, Hanyang University, Seoul 04763, Korea
* Correspondence: ywsuh@hanyang.ac.kr

Abstract: The selective transformation of secondary alcohols to alpha-olefins is a challenging task in heterogeneous catalysis, as is the case of 4-methyl-2-pentanol (4M2Pol) conversion to 4-methyl-1-pentene (4M1P). Herein, the co-precipitated yttria-stabilized zirconia (YSZ) catalysts exhibit superior performance to both bare and Y-impregnated ZrO_2 in selective 4M2Pol dehydration. In order to track the activity origin of YSZ, temperature-programmed desorption experiments using NH_3 and CO_2 are performed along with X-ray photoelectron spectroscopy. The conversion of 4M2Pol (max. 85%) is proportional to weak acidity and inverse to medium basicity. In contrast, the selectivity of 4M1P increases to 80% as the ratio of weak acidity to medium basicity is close to and exceeds the unity. These indications corroborate that the balanced acid–base pair of YSZ leads to the selective formation of 4M1P from 4M2Pol, which is caused by strong interaction between zirconia and yttria in the YSZ. Additionally, the dehydration activity over YSZ of 4 mol% yttrium is sustained at 450 °C for 50 h. Therefore, the YSZ, which is often used for electrocatalysis, is believed to be a promising catalyst in the dehydration of 4M2Pol and, further, secondary alcohols.

Keywords: 4-methyl-2-pentanol; dehydration; alpha olefin; acid–base pair; yttria-stabilized zirconia

Citation: Lee, J.-H.; Kim, M.; Lim, S.; Mishra, D.K.; Suh, Y.-W. Yttria-Stabilized Zirconia of Balanced Acid-Base Pair for Selective Dehydration of 4-Methyl-2-pentanol to 4-Methyl-1-pentene. *Catalysts* **2022**, *12*, 559. https://doi.org/10.3390/catal12050559

Academic Editor: Guozhu Chen

Received: 4 May 2022
Accepted: 17 May 2022
Published: 19 May 2022

1. Introduction

Polymethylpentene (PMP) is a well-known thermoplastic polymer under the trade name TPX^{TM}, which exhibits low density, high melting point, excellent flexibility, and high transparency [1,2]. The PMP is manufactured by polymerization of 4-methyl-1-pentene (4M1P) that is conventionally derived from dimerization of propylene over a well-known Ziegler–Natta catalyst [3]. As an alternative to producing the branched α-olefin 4M1P, the dehydration of 4-methyl-2-pentanol (4M2Pol) deserves practical consideration because 4M2Pol can be synthesized from surplus acetone available in the chemical industry. Thus, it has been a long-term and challenging subject to dehydrate 4M2Pol to 4M1P selectively. Typical acid catalysts produce 4-methyl-2-pentene (4M2P) of *cis* and *trans* isomers in large amounts, while 4-methyl-2-pentanone (4M2Pon) can sometimes be formed by dehydrogenation of 4M2Pol. In this respect, the dehydration of 4M2Pol is such a good model reaction in discerning the strength and density of acid and base sites in binary metal oxides and their composites for the desired product distribution.

Cutrufello et al. [4] investigated the activity and product selectivity of zirconium, cerium, and lanthanum oxides in 4M2Pol dehydration. When the ratio of surface acid to base sites was close to the unity ($n_B/n_A = 1$), the 4M1P selectivity of around 80% was achieved owing to the reaction progress via the E1cB mechanism. However, the larger number of base sites ($n_B/n_A > 1$) promoted the dehydrogenation of 4M2Pol to 4M2Pon, whereas the opposite case (i.e., $n_B/n_A < 1$) preferred the dehydration of 4M2Pol to 4M2P.

The works on the activities of silica-supported Ce_xZr_{1-x} catalysts revealed that the addition of Zr^{4+} to CeO_2 significantly increased the conversion of 4M2Pol with the improved 4M1P selectivity, resulting from the generation of acid–base surface sites [5,6]. However, the selectivity of 4M1P over these catalysts was lowered by the increase in reaction temperature, unlike the reactant conversion. This prompted to search for a new catalyst system for the balanced acid–base pair leading to high 4M1P selectivity at high temperatures.

Yttria-stabilized zirconia (YSZ) has proved to be a promising material in the field of electrochemistry because of its high ionic conductivity, high mechanical strength, and good thermal stability [7,8]. The YSZ has been accessed as a heterogeneous catalyst but is not well explored. Labaki et al. [9] examined the higher activity of CuO/YSZ catalysts in the oxidation of propylene and toluene due to the oxygen vacancies of YSZ involved in the oxidation mechanism catalyst. Vlasenko et al. [10] reported that the strong basicity and weak acidity of YSZ contributed to the high selectivity of *n*-butanol in the Guerbet coupling of ethanol. In glycerol stream reforming, the high performance of Ni-on-YSZ catalysts was attributed to the easy reducibility of NiO and the higher concentration of medium acid sites with fewer base sites compared to Ni/ZrO_2 [11]. Despite these potentials of YSZ in heterogeneous catalysis, there is a very limited number of reports to date, which is the motive of this study to investigate the catalytic activity and properties of YSZ in the dehydration of 4M2Pol to 4M1P.

Herein, YSZ catalysts with different yttrium contents are prepared by co-precipitation and also by incipient wetness impregnation for comparison. The prepared catalysts are evaluated in the dehydration of 4M2Pol at the temperature of 350, 375, and 400 °C. In order to figure out the obtained catalytic performance, the density and strength of acid and base sites are examined by temperature-programmed desorption experiments using NH_3 and CO_2 as probe molecule, which are thereafter correlated with the reactant conversion and product selectivities. Furthermore, the electron densities of YSZ's elements are characterized to address the changes in Lewis acidity and basicity. Through a series of these works, it can be addressed that the balanced acid–base pair of YSZ greatly contributes to the selective activation of 4M2Pol to 4M1P owing to a strong interaction between zirconia and yttria in the YSZ.

2. Results and Discussion

2.1. Physical Properties of YSZ Catalysts

From the results of N_2 physisorption, the specific surface area was calculated by the Brunauer-Emmett-Teller (BET) method. The BET surface area (S_{BET}) of *t*-ZrO_2 was measured at 42 $m^2\ g^{-1}$. The addition of 4% yttrium to *t*-ZrO_2 (4YSZ) increased the S_{BET} to 58 $m^2\ g^{-1}$, and further addition of up to 30% yttrium (30YSZ) decreased in a linear fashion to 18 $m^2\ g^{-1}$ (Figure 1). The pore volume (V_p) was decreased for the co-precipitated YSZ catalysts with higher yttrium contents. The co-precipitation generally results in homogeneous mixing of metal elements, such as Zr^{4+} and Y^{3+} in this work, which was confirmed in the field-emission scanning electron microscopy (FE-SEM) image of 20YSZ (Figure S1a). Therefore, the observed decreases in S_{BET} and V_p are caused by strong interaction between Zr^{4+} and Y^{3+} due to charge imbalance. In contrast, the impregnated catalysts 4Y/*t*-ZrO_2 and 20Y/*t*-ZrO_2 showed lower S_{BET} and V_p than bare *t*-ZrO_2 because the yttria existed on the external surface of *t*-ZrO_2 (Figure S1b) thereby blocking some pores at the surface.

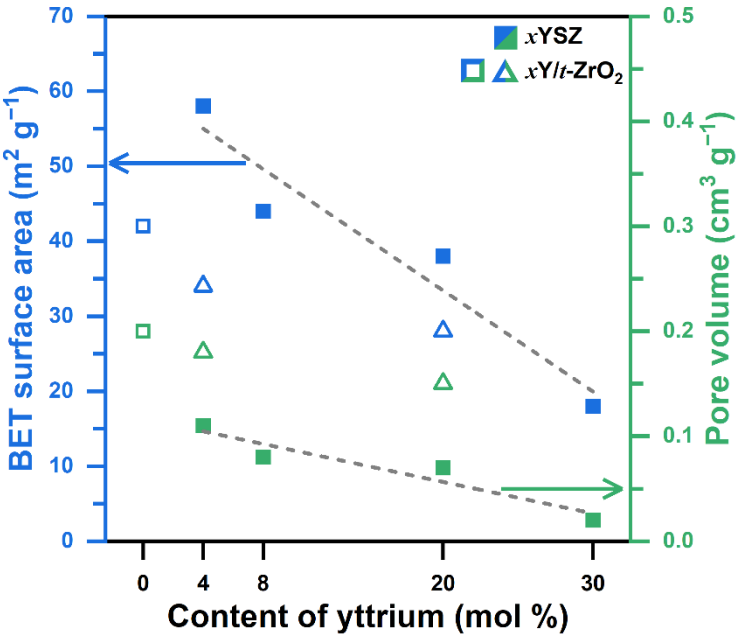

Figure 1. BET surface areas and the pore volumes of the co-precipitated xYSZ (filled squares) and impregnated xY/t-ZrO_2 (open triangles) catalysts along with bare t-ZrO_2 (open squares).

The crystallinity of the fresh YSZ catalysts was examined by X-ray diffraction (XRD) analysis. The diffraction peaks of t-ZrO_2 were detected at the 2θ angles of 30.3°, 50.5°, and 60.0°. These peaks were identically found in the patterns of 4YSZ and 8YSZ (Figure 2a). However, the major diffraction peak was shifted to a lower 2θ angle of 29.9° for 20YSZ and 30YSZ, indicating the formation of the cubic phase. The previous reports confirmed that the YSZ with the yttrium content of higher than 8% exhibits the transition from tetragonal to cubic phase because lattice distortion occurs by the incorporation of Y^{3+} into t-ZrO_2 [12,13]. However, the diffraction peaks of monoclinic ZrO_2 were additionally seen with no peak shift of t-ZrO_2 in the patterns of the impregnated catalysts 4Y/t-ZrO_2 and 20Y/t-ZrO_2 (Figure 2b). This suggests that the structure of t-ZrO_2 is changed by the existence of Y_2O_3 at the surface of particles. Furthermore, the diffraction at 29.3° was found in the pattern of 20Y/t-ZrO_2, which was assigned to the cubic phase of Y_2O_3 (JCPDS card no. 89-5591). Therefore, the co-precipitation leads to the well-mixing of Zr^{4+} and Y^{3+} in the oxide lattice, unlike the impregnation.

2.2. Catalytic Dehydration Performance of YSZ Catalysts

The co-precipitated YSZ and impregnated Y/t-ZrO_2 catalysts along with bare t-ZrO_2 were tested in the continuous reactor for the dehydration of 4M2Pol. As the reaction temperature increased from 350 to 400 °C, the conversion of 4M2Pol was improved for all of the tested catalysts. Because the catalyst rank was unchanged at each temperature, the catalytic activity and product selectivity at 400 °C were discussed. The t-ZrO_2 showed a 39% conversion of 4M2Pol with a low selectivity of 4M1P (20%) and high selectivity of 4M2Pon (78%). In the case of the impregnated catalysts, the conversion was declined to 29% and 27% for 4Y/t-ZrO_2 and 20Y/t-ZrO_2, respectively, whereas the opposite trend was seen in the selectivity of 4M1P. This is the effect of Y_2O_3 located at the surface of t-ZrO_2.

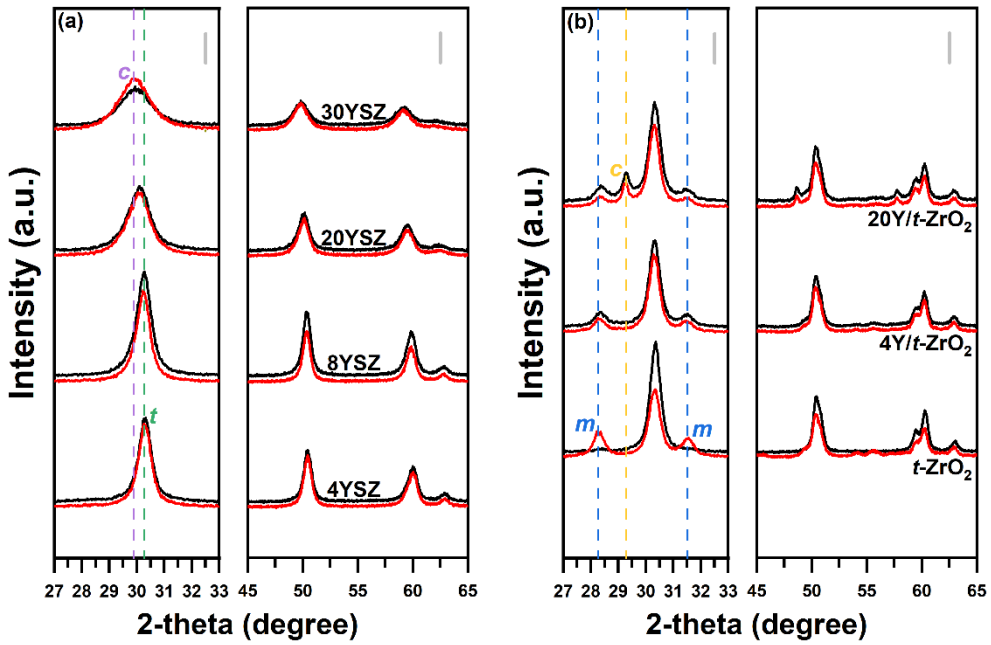

Figure 2. XRD patterns of the fresh (black lines) and spent (red lines) catalysts. (**a**) *x*YSZ (*x* = 4, 8, 20, and 30). (**b**) *x*Y/*t*-ZrO_2 (*x* = 4 and 20) and bare *t*-ZrO_2. The dot lines marked in purple, green, blue, and yellow represent the reflections of *c*-ZrO_2, *t*-ZrO_2, *m*-ZrO_2, and *c*-Y_2O_3, respectively.

In contrast, 4YSZ and 8YSZ presented a much higher 4M2Pol conversion (ca. 80% and 85%, respectively) than *t*-ZrO_2 (Figure 3a), representing that the former catalysts are intrinsically different from the latter, possibly because of the stabilization of *t*-ZrO_2 by the presence of yttria. However, the conversion of 4M2Pol over 20YSZ and 30YSZ was decreased to 64% and 52%, respectively, which may be associated with the reduced textural properties and other parameters of these catalysts. More importantly, the selectivity of 4M1P over the co-precipitated YSZ catalysts was in the range of 75–79% at 400 °C (Figure 3b), which was much higher than those over the impregnated Y/*t*-ZrO_2 ones affording 4M2Pon as the major product (Figure 3c). The favorable formation of 4M2Pon over Y/*t*-ZrO_2 was confirmed by the dehydration results at 350 and 375 °C (Figure S2). Moreover, the selectivity of 4M1P over 20YSZ and 30YSZ was decreased by increasing the reaction temperature from 350 to 450 °C (Figure S3). The measured product selectivity manifests that the dominant pathway is different over the YSZ and Y/*t*-ZrO_2 catalysts. Generally, the conversion of 4M2Pol to 4M1P follows the E1cB mechanism, whereas 4M2P and 4M2Pon are formed via E1 and dehydrogenation mechanisms, respectively. In other words, the distribution of 4M2Pol dehydration products depends upon the acidity and basicity of catalysts. In addition, the ratio of *cis*- to *trans*-4M2P was higher for *t*-ZrO_2 and Y/*t*-ZrO_2 than for YSZ (Figure S4). Hattori [14] reported that the *cis*/*trans* ratio of 2-alkene was high for base catalysts and close to the unity for acid catalysts. This allows speculating that the impregnated Y/*t*-ZrO_2 are more basic than the co-precipitated YSZ. When the conversion of 4M2Pol was plotted against the selectivity of 4M1P from the results at 400 °C, all of the YSZ catalysts were positioned at the upper right corner, unlike *t*-ZrO_2 and Y/*t*-ZrO_2 (Figure 3d). This indicates that the acid–base characters of the former catalysts are more favorable to selective dehydration of 4M2Pol into 4M1P compared to the latter ones.

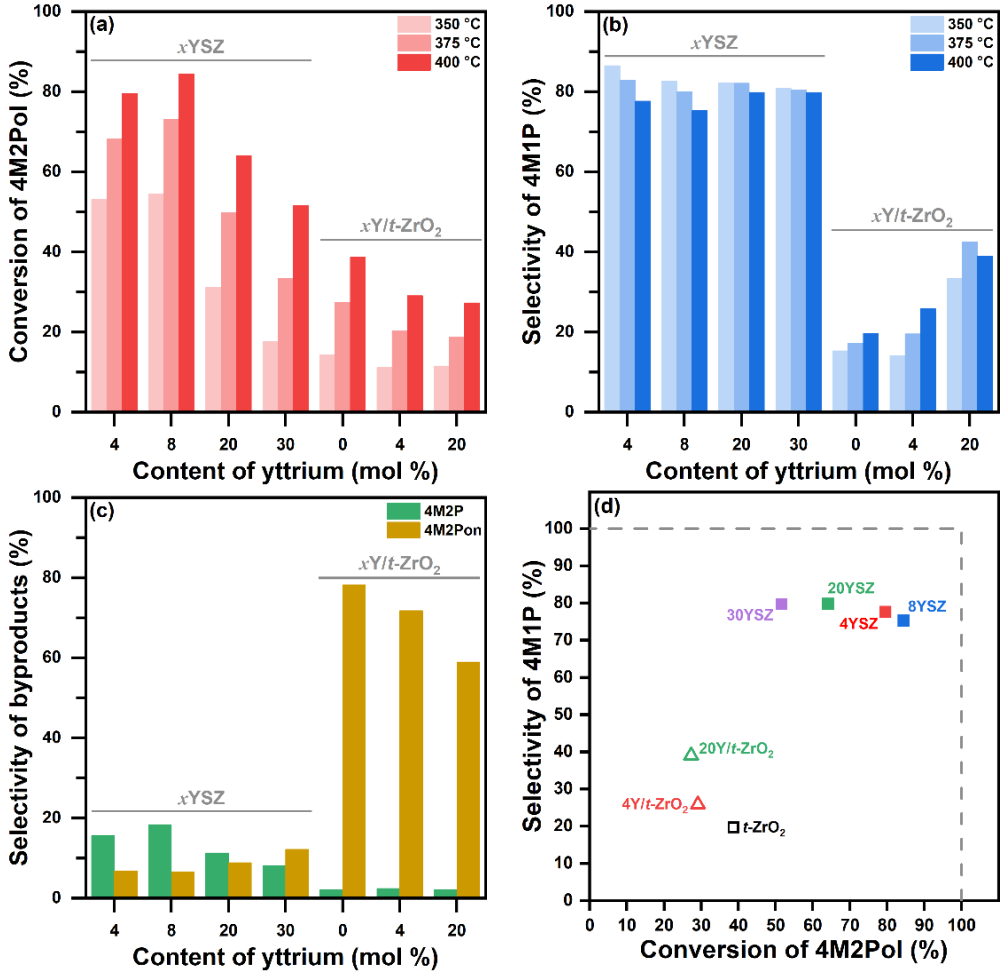

Figure 3. Activity results in dehydration of 4M2Pol over the co-precipitated *x*YSZ (*x* = 4, 8, 20, and 30) and impregnated *x*Y/*t*-ZrO_2 (*x* = 4 and 20) catalysts along with bare *t*-ZrO_2. (**a**) Conversion of 4M2Pol at 350, 375, and 400 °C. (**b**) Selectivity of 4M1P at 350, 375, and 400 °C. (**c**) Selectivity of by-products such as 4M2P and 4M2Pon at 400 °C. (**d**) Plot to correlate 4M2Pol conversion with 4M1P selectivity obtained at 400 °C.

Isothermal activity tests at 450 °C were performed with 4YSZ and 4Y/*t*-ZrO_2. In the tests for 50 h, 4YSZ showed stable performance, such as 82% conversion of 4M2Pol and 82% selectivity of 4M1P (Figure 4). However, the conversion of 4M2Pol over 4Y/*t*-ZrO_2 was dropped from 50% to 33% at time-on-stream of 50 h, while the selectivity of 4M1P was maintained at a low value of 35%. Furthermore, the diffraction patterns of the fresh and spent catalysts were compared. The change in peak intensity was apparent on 20YSZ and 30YSZ but not on 4YSZ and 8YSZ, of which thermal stability was ascribed to the stabilizer role of yttria in YSZ [15]. In the case of the spent 4Y/*t*-ZrO_2 and 20Y/*t*-ZrO_2, the phase transition from tetragonal to monoclinic ZrO_2 and the formation of cubic Y_2O_3 were observed. This explains the decrease in the conversion of 4M2Pol.

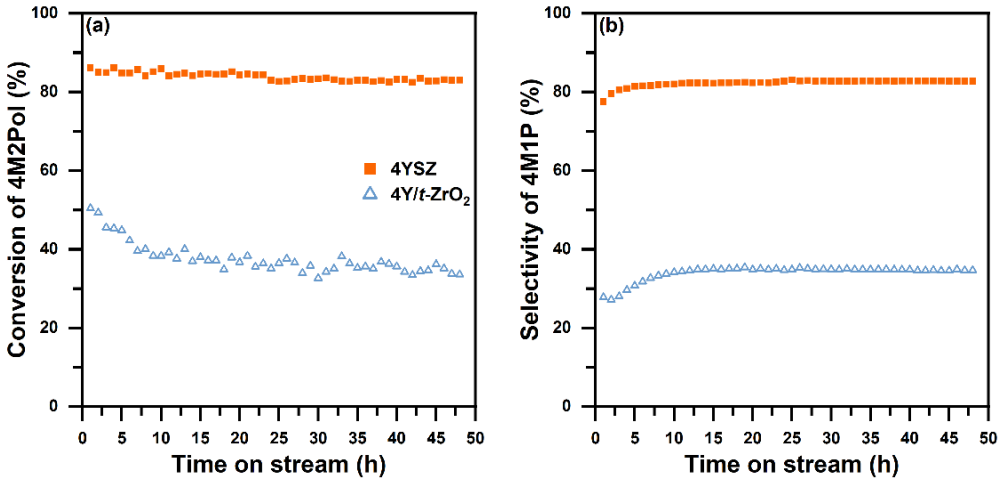

Figure 4. Long-term activity test at 450 °C for 50 h over 4YSZ and 4Y/*t*-ZrO_2. (**a**) Conversion of 4M2Pol. (**b**) Selectivity of 4M1P.

2.3. Acid–Base Characters of YSZ Catalysts

The density and strength of acid and base sites were measured by temperature-programmed desorption (TPD) experiments using the probe molecule of basic NH_3 and acidic CO_2, where yttria (Y_2O_3) was prepared by precipitation for comparison. TPD profiles were deconvoluted by the Gaussian function, as shown in Figure 5. Among the characterized catalysts, *t*-ZrO_2 showed the smallest NH_3-TPD profile at low temperatures (Figure 5a), meaning the smallest and weakest acidity of *t*-ZrO_2. The comparable acidity was observed with 20Y/*t*-ZrO_2 showing the formation of cubic Y_2O_3 particles (revealed by XRD analysis). However, the acidity was increased by the addition of 4% yttrium into *t*-ZrO_2 via impregnation. This is likely caused by good dispersion of yttria particles at the surface of *t*-ZrO_2 and, accordingly, the possible formation of Y–O–Zr linkage, which was confirmed in the NH_3-TPD profiles of the co-precipitated YSZ catalysts with increasing the yttrium content. The weak acidity was pronounced for 4YSZ and 8YSZ by incorporation of Y_2O_3, and then the strong acidity was generated for 20YSZ and 30YSZ. Thus, the higher the yttrium content, the larger the total acidity. Table 1 summarizes the calculated density of acid sites in a unit of μmol m^{-2}, where those of weak, medium, and strong acidity were determined in NH_3 desorption detected below 275 °C, between 275 and 550 °C, and above 550 °C, respectively, which refers to the reports on zirconia-based catalysts [16,17].

Table 1. Density of acid and base sites for all of the tested catalysts.

Catalyst	Acid Sites (μmol m^{-2})				Base Sites (μmol m^{-2})			
	Weak [a]	Medium [b]	Strong [c]	Total	Weak [d]	Medium [e]	Strong [f]	Total
20Y/*t*-ZrO_2	0.06	-	-	0.06	0.06	0.33	0.12	0.51
4Y/*t*-ZrO_2	0.10	0.03	0.09	0.22	0.06	0.26	0.04	0.37
t-ZrO_2	0.03	-	-	0.03	0.05	0.20	-	0.25
4YSZ	0.25	0.06	-	0.31	0.09	0.05	-	0.14
8YSZ	0.30	0.01	-	0.31	0.11	0.06	-	0.17
20YSZ	0.24	0.16	0.02	0.42	0.09	0.09	-	0.18
30YSZ	0.14	0.20	0.13	0.47	0.08	0.11	0.01	0.19

[a] Desorption above 275 °C. [b] Desorption between 275 and 550 °C. [c] Desorption above 550 °C. [d] Desorption below 150 °C. [e] Desorption between 150 and 550 °C. [f] Desorption above 550 °C.

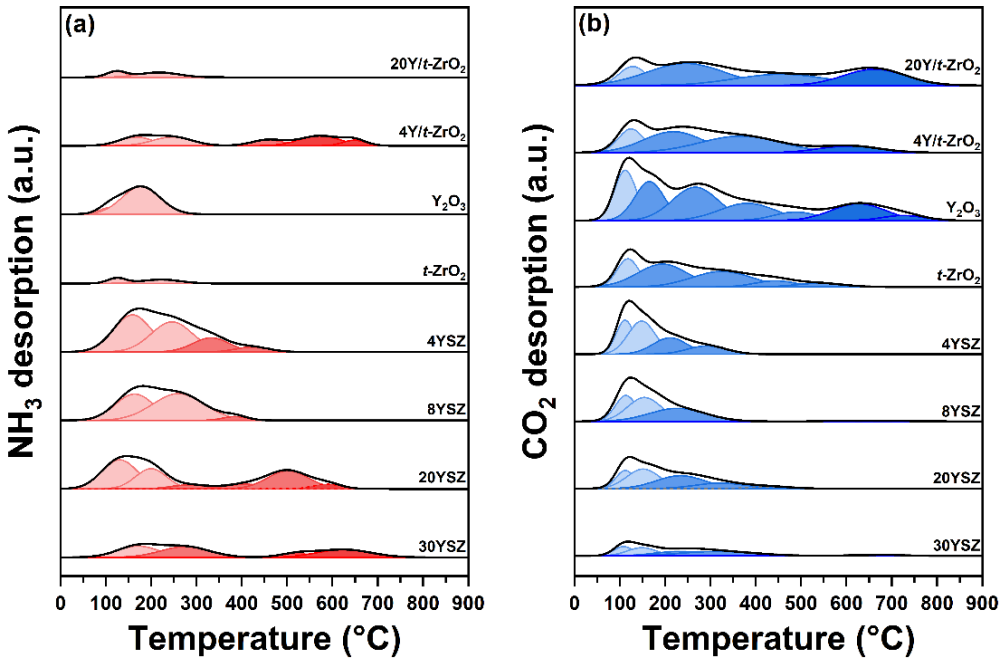

Figure 5. TPD profiles of (**a**) NH_3 and (**b**) CO_2 for the co-precipitated *x*YSZ (*x* = 4, 8, 20, and 30) and impregnated *x*Y/*t*-ZrO_2 (*x* = 4 and 20) catalysts along with bare *t*-ZrO_2. The deconvoluted peaks are distinguished by changing the intensity of red (**a**) and blue (**b**) colors from bright to dark with the desorption temperature increasing.

The CO_2-TPD profiles of *t*-ZrO_2 and Y_2O_3 identified that the basicity of Y_2O_3 was larger and stronger than that of *t*-ZrO_2 (Figure 5b), which was in agreement with the report of Paukshtis [18]. This finding was examined for 4Y/*t*-ZrO_2 and 20Y/*t*-ZrO_2, where the strong basicity was increased by the larger presence of basic Y_2O_3 at the surface of *t*-ZrO_2. In contrast, the desorption of CO_2 from YSZ catalysts was the major at temperatures of lower than 550 °C. Additionally, the integrated area of CO_2 desorbed per gram catalyst decreased with the increase in yttrium content. However, the total basicity per unit surface area increased for the YSZ with the higher yttrium content. The amount of CO_2 desorbed was used to calculate the density of base sites in a unit of μmol m^{-2} (Table 1), where the quantitative determination of weak, medium, and strong base sites was based upon the two distinct temperatures of 150 and 550 °C [16,17].

When the catalytic performance is considered in terms of the estimated values of acidity and basicity, the selective formation of 4M1P over the co-precipitated YSZ catalysts is associated with their weak and medium acid sites as well as weak and medium base sites. The pyridine-chemisorbed Fourier-transformed infrared (FT-IR) spectra of 4YSZ and 4Y/*t*-ZrO_2 revealed that Lewis acid sites, but not Brønsted acid sites, existed at the surface of the two catalysts (Figure S5). Thus, X-ray photoelectron spectroscopy (XPS) analysis was performed to distinguish the change of electron density using the core levels of Zr 3d, O 1s, and Y 3d, as presented in Figure 6. For comparison, the XPS spectrum of yttria was also obtained. In the Zr core level of *t*-ZrO_2, the peaks of Zr $3d_{3/2}$ and $3d_{5/2}$ were detected at the binding energy (BE) of 183.9 and 181.5 eV, respectively [19,20]. They were similarly observed in the spectrum of the impregnated Y/*t*-ZrO_2 (Figure S6). However, the co-precipitated YSZ showed the peak shift to higher BE by 0.3–0.4 eV compared to *t*-ZrO_2 (Figure 6a). This indicates the electron deficiency of Zr^{4+} centers that is equivalent to the increased Lewis acidity of YSZ, which can explain the presence of weak and medium acid sites in 4YSZ and 8YSZ. Meanwhile, the intensity of Zr $3d_{3/2}$ and $3d_{5/2}$ peaks was decreased in the YSZ with higher yttrium contents, thus increasing the atomic ratio of Y/Zr in the following order: 0.07 (4YSZ) < 0.13 (8YSZ) < 0.30 (20YSZ) < 0.41 (30YSZ). Therefore, another Lewis acidity would come from Y^{3+} centers. Figure 6b presents the Y $3d_{3/2}$ and $3d_{5/2}$ peaks of Y_2O_3 at 158.5 and 156.2 eV, respectively [21], which was also found in the

spectrum of 20Y/*t*-ZrO_2 (Figure S6). They were weak in 4Y/*t*-ZrO_2, 4YSZ, and 8YSZ, although they shifted to higher BE. However, 20YSZ and 30YSZ exhibited larger peaks along with the more BE shift, which was attributed to high substitution of yttrium in the matrix of *t*-ZrO_2 [12]. The XPS results observed in 20YSZ and 30YSZ indicate the formation of strong Lewis acid sites that is in agreement with the high-temperature NH_3 desorption.

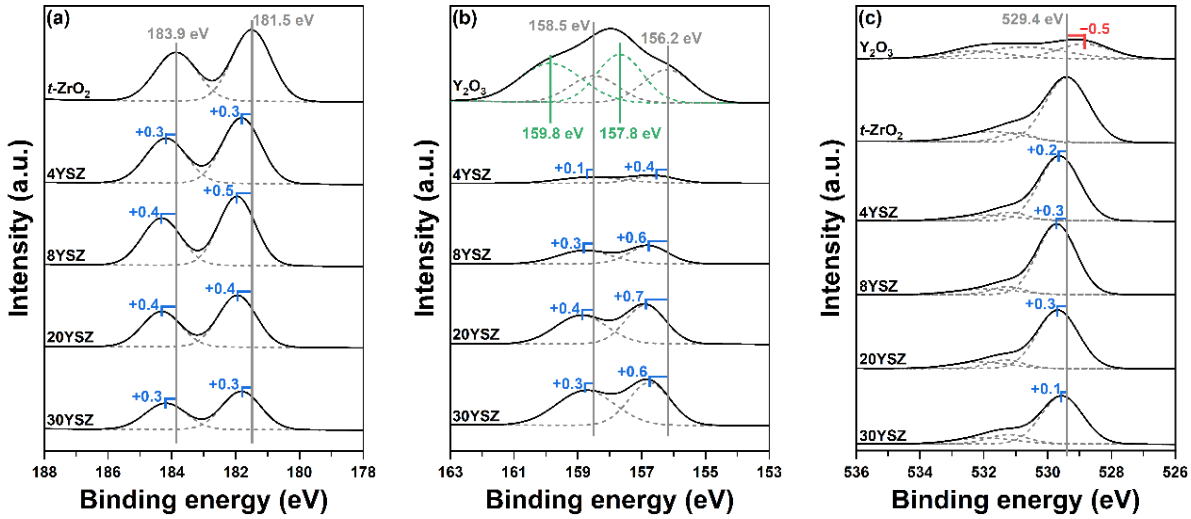

Figure 6. XPS spectra of the co-precipitated YSZ catalysts in the core levels of (**a**) Zr 3d, (**b**) Y 3d, and (**c**) O 1s. The spectra of *t*-ZrO_2 and/or Y_2O_3 are added for comparison.

On the other hand, the peak of O 1s at 529.4 eV is usually assigned to the surface lattice oxygen [22,23]. Such a peak was observed in the spectrum of *t*-ZrO_2 (Figure 6c). However, Y_2O_3 showed the signal of O 1s at a lower binding energy of 528.9 eV. This indicates the electron-rich state of oxygen species in Y_2O_3, representing strong Lewis base sites [12]. In addition, the shoulder peak in the core level of O 1s was clearly visible at around 532 eV. This is assigned to the oxygen anion of the hydroxyl group of $Y(OH)_3$, while the peaks of Y 3d at 157.8 and 159.8 eV (Figure 6b) confirmed the existence of $Y(OH)_3$ [21,24]. The oxygen species of $Y(OH)_3$ functions as Lewis base sites [25,26]. In contrast, the peak of O 1s was shifted to higher BE for the co-precipitated YSZ, which strongly suggested that the strong basicity of Y_2O_3 was weakened by the well-mixing with ZrO_2. This is in good agreement with the NH_3-TPD results of YSZ catalysts. Consequently, the acid–base pair of YSZ catalysts is explained by the electron-withdrawing action responsible for the increase in Lewis acidity of Zr^{4+} and Y^{3+} centers as well as the decrease in Lewis basicity of oxygen anion.

2.4. Understanding of Active Sites of YSZ Catalysts for 4M2Pol Dehydration

Based on the density and strength of acidity and basicity measured by TPD experiments, we attempted correlating them with the conversion of 4M2Pol. Figure 7 presents that the conversion of 4M2Pol is greatly affected by the two parameters such as weak acidity and medium basicity. The density of weak acid sites is in proportional relationship with the catalytic activity, but that of total acid sites is not the case. This corroborates that the weak acid sites play an important role in increasing the conversion of 4M2Pol. On the contrary, the conversion of 4M2Pol is inversely related to the density of medium base sites. This tendency is also seen in the density of total base sites because the contribution of weak base sites is not large (Figure S7). Therefore, the reduced density of medium base sites is preferable to the enhanced dehydration of 4M1Pol. When the above discussion is considered together, the weak acidity and medium basicity of the co-precipitated YSZ catalysts are key factors in activating the reactant 4M2Pol for the dehydration reaction.

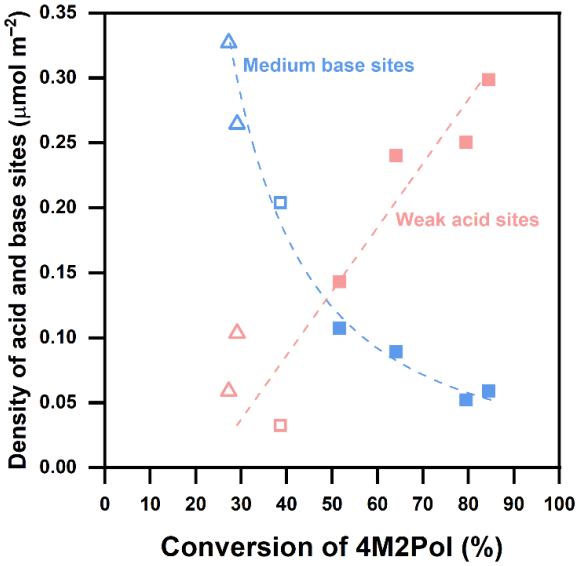

Figure 7. Correlation of 4M2Pol conversion with the surface density of weak acid sites and medium base sites for *x*YSZ (filled squares), *x*Y/*t*-ZrO_2 (open triangles), and bare *t*-ZrO_2 (open squares).

Similar approaches were performed to determine the factors affecting the selectivity of the desired product 4M1P. Because this selectivity failed to be correlated with each density of acid and base sites listed in Table 1, the surface density ratios of acidity to basicity were calculated and then correlated with the selectivity of 4M1P (Figure S8). As a result, the ratio of weak acidity to medium basicity (denoted as n_{WA}/n_{MB}) turned out to show the best fit to the 4M1P selectivity (Figure 8). In detail, the selectivity of 4M1P was increased and then saturated above the n_{WA}/n_{MB} close to the unity. This is in partial accordance with the report of Cutrufello et al. [4] that the 4M1P selectivity of around 80% was achieved when the ratio of total acid and base sites was close to the unity, whereas the larger number of total acid sites preferred the dehydration of 4M2Pol to 4M2P. The discrepancy with their work would be attributed to our detailed analysis of the density and strength of acid and base sites. In addition, the n_{WA}/n_{MB} was well correlated with the selectivities of 4M2P and 4M2Pon: as the n_{WA}/n_{MB} increased to 5, the former byproduct was more formed up to 20% in a linear fashion, and the latter byproduct was less formed and (Figure 8). This means that the n_{WA}/n_{MB} determines the selectivities of all the dehydration products. Therefore, the product distribution in the dehydration of 4M2Pol relies on the balanced acid–base pair of the co-precipitated YSZ catalysts.

Finally, the plausible reaction mechanism is discussed for the dehydration of 4M2Pol to 4M1P, 4M2P, and 4M2Pon over the YSZ catalysts. The 4M2Pol adsorbed on the catalyst surface undergoes the elimination reaction to 4M1P and 4M2P through E1cB and E1 mechanisms, respectively, and the dehydrogenation reaction to 4M2Pon. In the first step of the E1cB mechanism (Figure 9), the oxygen and hydrogen atoms in the hydroxyl (–OH) group of 4M2Pol are bonded to the Lewis acid sites (Zr^{4+}) and Lewis base sites (O^{2-}) on the surface of YSZs while another base sites withdraw the most acidic α-hydrogen of the methyl group, leading to the formation of an electron-rich carbanion intermediate. The electron in this carbanion is transferred to adjacent carbon, followed by pushing the bonding electron of the carbon toward the O bonded to Zr. Hence, the double bond is formed at the terminal position like 4M1P (Hoffman product). In the case of the E1 mechanism, the formation of 4M2P occurs on the Lewis acid sites attracting the electron from the oxygen of hydroxyl groups, followed by partitioning the electron of the C–H bond into the oxygen anion of the metal oxide (Figure S9a). This sequence yields first a carbocation intermediate and then 4M2P. This is in accordance with the increased selectivity of 4M2P by virtue of the higher weak acidity of the YSZ catalyst. On the other hand, the formation of 4M1Pon through the dehydrogenation pathway takes place at Lewis base sites (O^{2-}) on the surface of Y_2O_3

rather than on the amphoteric surface of YSZ, where the hydrogen atom of the hydroxyl group interacts with Lewis base sites involving the formation of carbanion and rupture of C–H bond, finally releasing 4M2Pon and H_2 (Figure S9b).

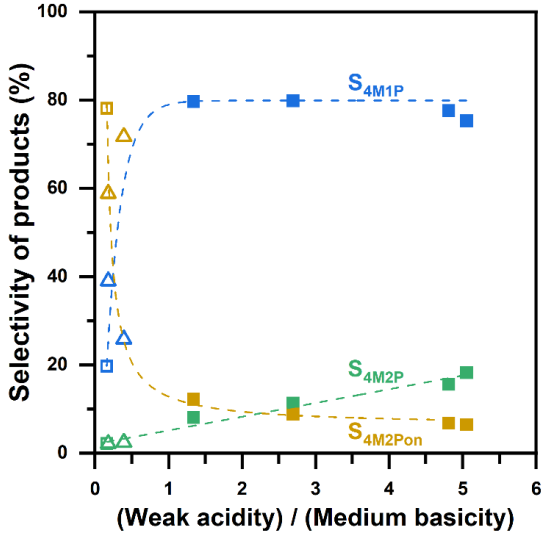

Figure 8. Correlation of product selectivity (S_{4M1P}, S_{4M2P}, and S_{4M2Pon}) with the surface density ratio of weak acidity to medium basicity for *x*YSZ (filled squares), *x*Y/*t*-ZrO_2 (open triangles), and bare *t*-ZrO_2 (open squares).

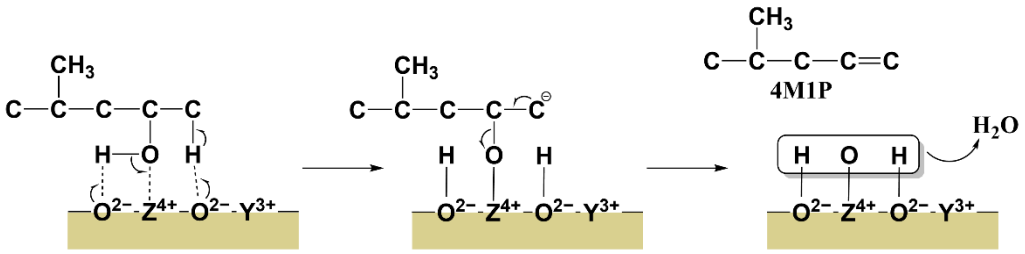

Figure 9. Plausible reaction mechanism on the conversion of 4M2Pol into 4M1P via E1cB pathway over the YSZ catalyst.

3. Materials and Methods

3.1. Preparation of Yttria-Stabilized Zirconia

For co-precipitation, an aqueous solution of ammonium hydroxide (NH_4OH, 25%) as the precipitating agent was added dropwise to a 1.2 M aqueous solution of $ZrO(NO_3)_2{\cdot}xH_2O$ (≥97.0%, Strem Chemicals, Newburyport, MA, USA) and $Y(NO_3)_3{\cdot}6H_2O$ (99.8%, Sigma-Aldrich, Munich, Germany) under stirring at 400 rpm. Then, the suspension was aged at 70 °C for 90 min. The resulting precipitate was filtered and washed four times with distilled water, followed by drying at 105 °C overnight. Finally, the dried sample was calcined at 750 °C for 5 h. This sample is named *x*YSZ, in which *x* is the yttrium content of 4, 8, 20, and 30 in a unit of mole percentage.

The conventional impregnation was performed to afford the catalysts yttria supported on tetragonal zirconia. Thus, a NaOH solution of 0.24 M was added dropwise to a 1.2 M aqueous solution of $ZrO(NO_3)_2{\cdot}xH_2O$ under stirring at 400 rpm, followed by aging at 70 °C for 90 min, filtering, and washing four times with distilled water. Then, the sample was dried at 105 °C overnight and calcined at 600 °C for 5 h to acquire tetragonal zirconia (*t*-ZrO_2). To the prepared *t*-ZrO_2 (1 g), an aqueous $Y(NO_3)_3{\cdot}6H_2O$ solution of 1.1 M was impregnated. The resulting sample was dried at 105 °C for 12 h and calcined at 750 °C for 5 h. This catalyst is denoted as *x*Y/*t*-ZrO_2 (*x* = 4 and 20 in a unit of mole percentage).

3.2. Dehydration Experiments

The dehydration of 4M2Pol was performed in a fixed-bed reactor connected with a high-performance liquid chromatography (HPLC) pump, heating furnace, and sampling port. The prepared catalyst powder was pressed, crushed, and sieved to a mesh size of 650–800. Then, this sample was placed in the middle of a stainless-steel tubular reactor (10 mm inner diameter and 40 cm length). Prior to activity tests, the catalyst was pretreated in a flow of N_2 (122 cm^3 min^{-1}) at 500 °C for 2 h and then cooled to the desired reaction temperature from 275 to 400 °C for temperature-programmed and isothermal tests. The liquid reactant was fed at a flow rate of 0.03 mL min^{-1}) to the reactor while the N_2 flow was unchanged. The product stream was passed to a gas chromatograph (Agilent Technologies 7890B, Agilent Technologies, Santa Clara, CA, USA) equipped with an HP-1 capillary column and flame ionization detector. The moles of the unconverted reactant and formed products were measured and converted to determine the conversion of 4M2Pol and product selectivities.

3.3. Characterization

XRD patterns were recorded with a Rigaku MiniFlex 600 diffractometer. The specific surface area and pore volume were measured using a Micromeritics ASAP 2020 instrument after degassing at 150 °C in a vacuum for 1.5 h. FE-SEM images were taken in a JEOL 8700F microscope with an electron dispersive X-ray spectrometer. XPS analysis was performed using a Thermo Fisher Scientific (Thermo Fisher Scientific, Waltham, MA, USA) K-alpha spectrometer with a monochromatic Al Kα X-ray source operated at a voltage of 1486.6 eV and pass-energy of 200 eV, where the binding energy was calibrated with the standard C 1s signal of 248.6 eV. FT-IR analysis was conducted in a Thermo Nicolet 6700 spectrometer equipped with an MCT-A detector. The adsorption of pyridine was performed at 100 °C for 10 min after pretreatment at 100 °C in a vacuum for 1 h, followed by vacuum degassing to remove pyridine physisorbed. Pyridine-chemisorbed FT-IR spectra were taken in the range of 1700 to 1400 cm^{-1}. TPD experiments using NH_3 or CO_2 were conducted in a BELCAT-B instrument coupled with a mass spectrometer. After pretreatment at 500 °C in He for 2 h, a sample (550 mg) was cooled to 50 °C, exposed to a flow of 5% NH_3/He or 5% CO_2/He for 1 h, and purged in He for 30 min. Then, the sample was heated to 900 °C in a He flow of 30 cm min^{-1}.

4. Conclusions

The co-precipitated YSZ catalysts were first explored to selectively dehydrate 4M2Pol into 4M1P with a low abundance of 4M2P and 4M2Pon. The 4YSZ and 8YSZ exhibited the 4M2Pol conversion of higher than 80% and the 4M1P selectivity of 75–79% at 400 °C. Moreover, the dehydration performance of 4YSZ at 450 °C was maintained for 50 h, affording 82% conversion of 4M2Pol and 82% selectivity of 4M1P. The activity results corroborate the great potential of the YSZ catalysts in the selective conversion of 4M2Pol into 4M1P. This is attributed to the balanced acid–base pair of YSZ catalysts, unlike the impregnated Y/*t*-ZrO_2 catalysts. The TPD results examined that the homogeneous mixing of Zr^{4+} and Y^{3+} in the matrix of YSZ increased the weak acidity and reduced the strong base sites, which was supported by the measured XPS spectra. These features contributed to the selective formation of 4M1P from 4M2Pol. However, the acid-catalyzed dehydration to 4M2P and the base-catalyzed dehydrogenation to 4M2Pon occurred when the acid and base sites were imbalanced. Consequently, the strong interaction between zirconia and yttria in the YSZ is believed to induce the balanced acid–base pair favorable for the desired transformation of secondary alcohol 4M2Pol into branched α-olefin 4M1P.

Supplementary Materials: The following supporting information can be downloaded at: https://www.mdpi.com/article/10.3390/catal12050559/s1, Figure S1: FE-SEM images and elemental mapping images (O, Y, and Zr) of (a) 20YSZ and (b) 20Y/*t*-ZrO_2, Figure S2: Selectivity of by-products such as 4M2P and 4M2Pon in 4M2Pol dehydration at (a) 350 °C and (b) 375 °C, Figure S3: 4M2P conversion and product selectivity in 4M2Pol dehydration over (a) 20YSZ and (b) 30YSZ at 350 to 450 °C, Figure S4: Ratio of *cis*- to *trans*-4M2P at 350, 375, and 400 °C over the co-precipitated *x*YSZ (*x* = 4, 8, 20, and 30) and impregnated *x*Y/*t*-ZrO_2 (*x* = 4 and 20) catalysts along with bare *t*-ZrO_2, Figure S5: Pyridine-chemisorbed FT-IR spectra of the catalysts 4YSZ and 4Y/*t*-ZrO_2, Figure S6: XPS spectra of the impregnated Y/*t*-ZrO_2 catalysts in the core levels of (a) Zr 3d, (b) Y 3d, and (c) O 1s. The spectra of *t*-ZrO_2 and/or Y_2O_3 are added for comparison, Figure S7: Correlation of 4M2Pol conversion with the surface density of total acid sites, weak base sites, and total base sites of *x*YSZ (filled squares), *x*Y/*t*-ZrO_2 (open triangles), and bare *t*-ZrO_2 (open squares), Figure S8: Correlation of 4M1P selectivity with various surface density ratios. (a) Weak acidity to weak, medium, and total basicity. (b) Total acidity to weak, medium, and total basicity for *x*YSZ (filled squares), *x*Y/*t*-ZrO_2 (open triangles), and bare *t*-ZrO_2 (open squares), Figure S9: Plausible mechanism on the conversion of 4M2Pol. (a) Formation of 4M2P via E1 mechanism over YSZ. (b) Formation of 4M2Pon via dehydrogenation mechanism over YSZ.

Author Contributions: Data curation, J.-H.L. and M.K.; conceptualization, J.-H.L., M.K., S.L. and Y.-W.S.; methodology, J.-H.L. and M.K.; validation, J.-H.L., M.K. and S.L.; investigation, J.-H.L., M.K. and S.L. (J.-H.L.: material design, synthesis, and catalyst characterization, M.K.: catalyst characterization and catalytic experiments, S.L.: catalytic experiments); visualization, J.-H.L. and Y.-W.S.; supervision, Y.-W.S.; writing—original draft preparation, J.-H.L. and D.K.M.; writing—review and editing, J.-H.L., D.K.M. and Y.-W.S.; project administration, Y.-W.S.; funding acquisition, Y.-W.S. All authors have read and agreed to the published version of the manuscript.

Funding: This work was financially supported by the program titled "Technology Development Program to Solve Climate Changes" of the National Research Foundation of Korea under the Ministry of Science, ICT & Future Planning, Republic of Korea (NRF-2020M1A2A2080856), and by LG Chem, Ltd. (Contract No. 202100000002709). The author D.K.M. acknowledges the financial support of the Basic Science Research program through the National Research Foundation of Korea under the Ministry of Education, Republic of Korea (NRF-2016R1A6A1A03013422).

Conflicts of Interest: The authors declare no conflict of interest.

References

1. Kashiwa, N.; Fukui, K. Process for Production of 4-methyl-1-pentene Polymer or Copolymer. U.S. Patent No. 4,659,792, 21 April 1987.
2. Kashiwa, N.; Yoshitake, J. Polymerizations of α-olefins and styrene with $MgCl_2$-supported titanium catalyst system: $MgCl_2/TiCl_4/PhCO_2Et$ with $AlEt_3PhCO_2Et$. *Polym. Bull.* **1984**, *11*, 485–489. [CrossRef]
3. Lopez, L.C.; Wilkes, G.L.; Stricklen, P.M.; White, S.A. Synthesis, structure, and properties of poly(4-methyl-1-pentene). *J. Macromol. Sci. Part. C* **1992**, *32*, 301–406. [CrossRef]
4. Cutrufello, M.G.; Ferino, I.; Monaci, R.; Rombi, E.; Solinas, V. Acid-base properties of zirconium, cerium and lanthanum oxides by calorimetric and catalytic investigation. *Top. Catal.* **2002**, *19*, 225–240. [CrossRef]
5. Reddy, B.M.; Lakshmanan, P.; Bharali, P.; Saikia, P. Dehydration of 4-methylpentan-2-ol over $Ce_xZr_{1-x}O_2/SiO_2$ nano-composite catalyst. *J. Mol. Catal. A Chem.* **2006**, *258*, 355–360. [CrossRef]
6. Reddy, B.M.; Thrimurthulu, G.; Saikia, P.; Bharali, P. Silica supported ceria and ceria–zirconia nanocomposite oxides for selective dehydration of 4-methylpentan-2-ol. *J. Mol. Catal. A Chem.* **2007**, *275*, 167–173. [CrossRef]
7. Chen, X.J.; Khor, K.A.; Chan, S.H.; Yu, L.G. Influence of microstructure on the ionic conductivity of yttria-stabilized zirconia electrolyte. *Mater. Sci. Eng.: A* **2002**, *335*, 246–252. [CrossRef]
8. Shimonosono, T.; Ueno, T.; Hirata, Y. Mechanical and thermal properties of porous yttria-stabilized zirconia. *J. Asian Ceram. Soc.* **2019**, *7*, 20–30. [CrossRef]
9. Labaki, M.; Siffert, S.; Lamonier, J.-F.; Zhilinskaya, E.A.; Aboukaïs, A. Total oxidation of propene and toluene in the presence of zirconia doped by copper and yttrium: Role of anionic vacancies. *Appl. Catal. B Environ.* **2003**, *43*, 261–271. [CrossRef]
10. Vlasenko, N.V.; Kyriienko, P.I.; Valihura, K.V.; Kosmambetova, G.R.; Soloviev, S.O.; Strizhak, P.E. Yttria-stabilized zirconia as a high-performance catalyst for ethanol to n-butanol Guerbet coupling. *ACS Omega* **2019**, *4*, 21469–21476. [CrossRef]
11. Charisiou, N.D.; Siakavelas, G.; Tzounis, L.; Dou, B.; Sebastian, V.; Hinder, S.J.; Baker, M.A.; Polychronopoulou, K.; Goula, M.A. $Ni/Y_2O_3–ZrO_2$ catalyst for hydrogen production through the glycerol steam reforming reaction. *Int. J. Hydrogen Energy* **2020**, *45*, 10442–10460. [CrossRef]

12. Ohtsuka, S.; Nemoto, T.; Yotsumoto, R.; Yamada, Y.; Sato, F.; Takahashi, R.; Sato, S. Vapor-phase catalytic dehydration of butanediols to unsaturated alcohols over yttria-stabilized zirconia catalysts. *Appl. Catal. A Gen.* **2019**, *575*, 48–57. [CrossRef]
13. Vasanthavel, S.; Kannan, S. Structural investigations on the tetragonal to cubic phase transformations in zirconia induced by progressive yttrium additions. *J. Phys. Chem. Solids* **2018**, *112*, 100–105. [CrossRef]
14. Hattori, H. Solid base catalysts: Generation of basic sites and application to organic synthesis. *Appl. Catal. A Gen.* **2001**, *222*, 247–259. [CrossRef]
15. Ray, J.C.; Pati, R.K.; Pramanik, P. Chemical synthesis and structural characterization of nanocrystalline powders of pure zirconia and yttria stabilized zirconia (YSZ). *J. Eur. Ceram. Soc.* **2000**, *20*, 1289–1295. [CrossRef]
16. Albuquerque, E.M.; Borges, L.E.P.; Fraga, M.A.; Sievers, C. Relationship between acid–base properties and the activity of ZrO_2-based catalysts for the Cannizzaro reaction of pyruvaldehyde to lactic acid. *ChemCatChem* **2017**, *9*, 2675–2683. [CrossRef]
17. Wan Omar, W.N.N.; Amin, N.A.S. Biodiesel production from waste cooking oil over alkaline modified zirconia catalyst. *Fuel Processing Technol.* **2011**, *92*, 2397–2405. [CrossRef]
18. Glazneva, T.S.; Kotsarenko, N.S.; Paukshtis, E.A. Surface acidity and basicity of oxide catalysts: From aqueous suspensions to in situ measurements. *Kinet. Catal.* **2008**, *49*, 859–867. [CrossRef]
19. Bumajdad, A.; Nazeer, A.A.; Al Sagheer, F.; Nahar, S.; Zaki, M.I. Controlled synthesis of ZrO_2 nanoparticles with tailored size, morphology and crystal phases via organic/inorganic hybrid films. *Sci. Rep.* **2018**, *8*, 3695. [CrossRef]
20. Liu, G.X.; Liu, A.; Meng, Y.; Shan, F.K.; Shin, B.C.; Lee, W.J.; Cho, C.R. Annealing dependence of solution-processed ultra-thin ZrO*x* films for gate dielectric applications. *J. Nanosci. Nanotechnol.* **2015**, *15*, 2185–2191. [CrossRef]
21. Reddy, I.N.; Reddy, C.V.; Cho, M.; Kim, D.; Shim, J. Structural, optical, and XPS studies of doped yttria for superior water splitting under visible light illumination. *J. Electroanal. Chem.* **2019**, *848*, 113335. [CrossRef]
22. Gu, H.; Ding, J.; Zhong, Q.; Zeng, Y.; Song, F. Promotion of surface oxygen vacancies on the light olefins synthesis from catalytic CO_2 hydrogenation over FeK/ZrO_2 catalysts. *Int. J. Hydrog. Energy* **2019**, *44*, 11808–11816. [CrossRef]
23. Tan, J.; Cui, J.; Zhu, Y.; Cui, X.; Shi, Y.; Yan, W.; Zhao, Y. Complete aqueous hydrogenation of 5-hydroxymethylfurfural at room temperature over bimetallic RuPd/graphene catalyst. *ACS Sustain. Chem. Eng.* **2019**, *7*, 10670–10678. [CrossRef]
24. Cole, K.M.; Kirk, D.W.; Thorpe, S.J. $Y(OH)_3$ powder characterized by XPS. *Surf. Sci. Spectra* **2020**, *27*, 024007. [CrossRef]
25. Hadjiivanov, K. Identification and characterization of surface hydroxyl groups by infrared spectroscopy. In *Advances in Catalysis*; Jentoft, F.C., Ed.; Elsevier Inc.: Amsterdam, The Netherlands, 2014; Volume 57, pp. 99–318.
26. Puriwat, J.; Chaitree, W.; Suriye, K.; Dokjampa, S.; Praserthdam, P.; Panpranot, J. Elucidation of the basicity dependence of 1-butene isomerization on MgO/$Mg(OH)_2$ catalysts. *Catal. Commun.* **2010**, *12*, 80–85. [CrossRef]